HHS Public Access

Author manuscript

Neuroimage. Author manuscript; available in PMC 2022 February 15.

Published in final edited form as:

Neuroimage. 2022 February 15; 247: 118792. doi:10.1016/j.neuroimage.2021.118792.

Inside information: Systematic within-node functional connectivity changes observed across tasks or groups

Wenjing Luo[a], **R. Todd Constable**[a,b,c,*]

[a]Department of Biomedical Engineering, Yale University School of Medicine USA

[b]Radiology and Biomedical Imaging, Yale University School of Medicine USA

[c]Interdepartmental Neuroscience Program, Yale University School of Medicine USA

Abstract

Mapping the human connectome and understanding its relationship to brain function holds tremendous clinical potential. The connectome has two fundamental components: the nodes and the sconnections between them. While much attention has been given to deriving atlases and measuring the connections between nodes, there have been no studies examining the networks within nodes. Here we demonstrate that each node contains significant connectivity information, that varies systematically across task-induced states and subjects, such that measures based on these variations can be used to classify tasks and identify subjects. The results are not specific for any particular atlas but hold across different atlas resolutions. To date, studies examining changes in connectivity have focused on edge changes and assumed there is no useful information within nodes. Our findings illustrate that for typical atlases, within-node changes can be significant and may account for a substantial fraction of the variance currently attributed to edge changes .

1. Introduction

Since the concept of the human connectome was first introduced by Sporns in 2005 (Sporns et al., 2005), there has been tremendous interest in mapping the connectome and understanding its relationship to brain function in both the healthy and diseased brain. The connectome, whether it is constructed based on structural or functional connections (or both), requires two primary ingredients: the nodes and the connections between them. Once the nodes are defined, the connectome is constructed, by measuring the connections between

*Corresponding author. todd.constable@yale.edu (R.T. Constable).

Code and data availability

The Shen 268 atlas is available online on the BioImage Suite NITRC page (https://www.nitrc.org/frs/?group_id1451). The code for individualized parcellation is available in the publicly available Python package biswebpython: https://pypi.org/project/biswebpython/. Human Connectome Project (HCP) data (S900) are publicly available at https://www.humanconnectome.org/study/hcp-young-adult/document/1200-subjects-data-release.

Credit authorship contribution statement

Wenjing Luo: Conceptualization, Formal analysis, Investigation, Software, Validation, Writing – original draft, Writing – review & editing. **R. Todd Constable:** Conceptualization, Project administration, Resources, Supervision, Writing – review & editing.

Supplementary materials

Supplementary material associated with this article can be found, in the online version, at doi:10.1016/j.neuroimage.2021.118792.

all pairs of nodes. The connectome is a connectivity matrix, with both the rows and the columns representing the nodes, and the cells representing the strength of connection (called edges) between pairs of nodes. Magnetic resonance imaging (MRI) generally does not have directional information, and so the connectivity matrix is diagonally symmetric. The node is a fundamental component of the connectome, and these are usually defined by applying a brain atlas and averaging the BOLD time-course signals across all the voxels within each node prior to calculating the connectivity. Here we focus on functional connectivity (in contrast to structural connectivity) defined as the Pearson's r correlation of BOLD signals from pairs of nodes (Biswal et al., 1995). Once the connectivity matrix is obtained numerous approaches have been developed to measure changes in the connectome between groups and conditions, or in many cases graph theory approaches are applied to quantitatively summarize node and network properties (Rubinov and Sporns, 2010). With such measures, connectivity changes can be quantified between brain states and/or groups or as a function of some behavioral or clinical measure. Previous studies have shown correlations between functional connectivity and subject traits, such as sex (Satterthwaite et al., 2015; Zhang et al., 2016), age (Geerligs et al., 2015; Zhang et al., 2016), fluid intelligence (Finn et al., 2015b; Santarnecchi et al., 2017) and attention (Rosenberg et al., 2017, 2016, 2020). Network measures have also been related to subject features (Meunier et al., 2009; Rudie et al., 2013; Tian et al., 2011) and brain states (Cohen and D'Esposito, 2016; Shine et al., 2016).

While there is consensus on, and a large literature supporting, the application of graph theory to neuroimaging data, many methodological choices could affect such analyses. First there is no consensus on what to use for a brain atlas to define nodes. Secondly, unlike say disease propagation or the tracking of friends in social networks whether two nodes are connected (the disease was transmitted between individuals, or two people are or are not friends on Facebook, for example), neuroimaging data typically does not provide a binary framework easily defining whether two nodes are connected. While weighted graphs (Antoniou and Tsompa, 2008; Bolaños et al., 2013) can be constructed the most common approach is to binarized the connectivity matrix using an arbitrarily cutoff threshold to define a graph. Here we focus on subtleties associated with the application of an atlas to define the nodes and the information content within a node.

Parcellation of the cortex and subcortex is not only a key first step in defining nodes for network analysis. Because of the central importance of such atlases, brain parcellation has been an active area of research and a wide range of approaches and modalities have been used to attempt to define the ideal atlas (for a review see (Eickhoff et al., 2018)). While early atlases were based on cytoarchitecture (ala Brodmann (1909)) with the advent of 3D imaging approaches, atlases have been built based on morphometric information, white matter microstructure obtained through diffusion tensor imaging (DTI) MRI, myelography, task-based functional MRI, functional connectivity, and gene expression data. Recent work has yielded atlases based on individuals (Blumensath et al., 2013; Smith et al., 2013a), groups of subjects (Fan et al., 2016; Glasser et al., 2016; Gordon et al., 2016; Power et al., 2011; Shen et al., 2013; Yeo et al., 2011), based on anatomical MRI data (Caviness et al., 1996; Rolls et al., 2020), functional data (Gordon et al., 2016; Power et al., 2011; Shen et al., 2013; Yeo et al., 2011), or a combination of both (Fan et al., 2016; Glasser et

al., 2016). Atlases vary in their resolution (number of nodes in each atlas), coverage, and spatial perspective (volume-based or surface-based). The choice of atlas is somewhat critical as it has been shown that the results of functional connectivity analyses are atlas-dependent (Messé, 2020; Park et al., 2013) as are the results of network analysis (Lord et al., 2016; Park et al., 2013; Qi et al., 2015) when using functional connectivity data.

In addition to the lack of consensus on which atlas to use, recent work (Salehi et al., 2020) has highlighted how node boundaries defined by functional connectivity are flexible within a fixed anatomic framework. While it has long been known that there is sub-specialization in cortical regions, this raises two fundamental questions with respect to connectivity analyses: 1) Is there an ideal atlas for defining functional nodes; 2) Does it make sense to combine structural data (which is fixed at the functional time scale) with functional data which is dynamic and flexible in its organization. Node reorganization over short temporal windows has been demonstrated in non-overlapping whole-brain parcellations (Boukhdhir et al., 2021). There is considerable support for this flexible organization in the literature from studies using a variety of methods (Calhoun et al., 2008; Iraji et al., 2019; Ma et al., 2014; McIntosh, 2004; Yeo et al., 2015). Recent functional connectivity work has shown that quantitative results in graph theory measures when comparing groups of subjects or comparing the same subjects across different task-conditions, change significantly if node reconfiguration is taken into account through flexible individualized- or group- brain-state-dependent parcellations (Luo et al., 2021). Despite this knowledge, fixed atlases are still applied in most studies of the connectome, and the search continues for the ideal atlas (Bozek et al., 2018; Lawrence et al., 2021; Schaefer et al., 2018).

Fundamentally, the use of an atlas comes with the implicit assumption that the node functions as a uniform entity. If this assumption is wrong and within-node connectivity does change, such changes can be incorrectly interpreted as edge changes. Node homogeneity, defined as the mean pair-wise correlation between voxel-level time series within the node, is in fact often used as a measure of goodness of parcellation with better parcellations having higher within node homogeneity. Maximal node homogeneity is achieved when the time-courses of the voxels within the node are all very similar, which would be the case with uniform neural activity throughout the node.

In this work we demonstrate that the neural activity is far from uniform in most nodes, and most importantly, that the homogeneity changes systematically with tasks. For a given atlas one can create a homogeneity vector of length equal to the number of nodes in the atlas. Using this vector we show, across a range of atlases, that there is considerable information in the vector and that there are reliable task-dependent changes in connectivity within the nodes defined by typical atlases. Previous work showed that with a flexible functional parcellation approach a node size vector provided a measure that could be used to predict both the corresponding task during which the data were recorded as well as in-magnet task performance (Salehi et al., 2020). Here, across a selection of fixed atlases, we use node homogeneity to summarize between-voxel connectivity within-nodes and demonstrate that there is significant connectivity information contained within a node. The conclusion is that if one is interested in how functional connections in the brain change between tasks or

groups, then all such changes (including within node changes) should be considered, and analyses should not be limited to only the possibility of edge changes.

2. Methods

2.1. Data

A subset of the Human Connectome Project (HCP) S900 release was used. Only subjects who had voxel-level fMRI data for all nine functional sessions (two resting-states and seven tasks) with left-right phase-encoding were included. To alleviate artifacts caused by head motion, subjects with mean frame-to-frame displacement > 0.1 mm or maximum frame-to-frame displacement > 0.15 mm were excluded. The resulting dataset contains 493 subjects (266 females, age = 22–36+, subject IDs listed in supplementary material). The preprocessing procedures were the same as described in (Salehi et al., 2020). We applied the HCP minimal preprocessing pipeline (Glasser et al., 2013) which includes artifact removal, motion correction, and registration to MNI space. All further preprocessing steps used BioimageSuite (Joshi et al., 2011), including regressing 24 motion parameters, regressing the mean time courses of the white matter and cerebrospinal fluid, and the global signal, removing the linear trend and low pass filtering.

2.2. Brain atlases and parcellations

Three different functional atlases were used to investigate whether the results depend on atlas choice. Shen 268 is a 268-parcel atlas determined with a spectral clustering algorithm on resting-state data of a healthy population (Shen et al., 2013). Shen 368 is a finer atlas obtained by integrating the parcellation of cortex from (Shen et al., 2013), subcortex from the anatomical Yale Brodmann Atlas (Lacadie et al., 2008), and cerebellum from Yeo et al. (2011). Yeo 1041 was obtained by integrating the subcortical and cerebellum parcellation of the 368-parcel parcellation with the 1000-parcel cortex parcellation from Yeo et al. (2011). Another recent functional atlas Schaefer 400 (Schaefer et al., 2018) was used to further validate the results (Supplementary Fig. S3).

The exemplar-based individualized parcellation method previously proposed in (Salehi et al., 2020) was used to generate the individualized parcellations for each scan. The algorithm has three steps: 1) Registration to a group-level parcellation. Here we used the Shen 268 atlas as the initial group-level parcellation. 2) Identification of an exemplar from each node by maximizing a submodular function. 3) Assignment of each voxel to the functionally closest exemplar while maintaining spatial contiguity to an exemplar.

The state-specific parcellations were determined by taking the majority vote over the individualized parcellations for all the subjects during the same task. For example, a voxel in the working memory parcellation is assigned to the node to which the voxel is most frequently assigned across all 493 subject-specific working memory individualized parcellations.

Based on the nine state-specific parcellations, we obtained an intersect parcellation which only contains voxels that are assigned to the same node across all state-specific parcellations. Ambiguous voxels which are assigned to different nodes under different states

were not included in this parcellation leaving uncovered gaps between nodes. The intersect parcellation covers approximately 79% of the voxels covered in the resting- state-specific parcellation.

2.3. Homogeneity

We used node homogeneity to summarize between-voxel connectivity within-nodes and investigated how it changes across states and subjects. The homogeneity of each node is defined as the mean z-scored pair-wise correlation between voxel-level time series within the node. There is a homogeneity vector associated with each scan which contains the homogeneities of all the nodes defined by the atlas applied. The dimension of a homogeneity vector depends on the resolution of the atlas. (Fig. 1a) Six sets of homogeneity vectors were computed based on different atlases (Shen 268, Shen 368, Yeo 1041, state-specific parcellations, individualized parcellations, and intersect parcellation).

2.4. Task classification using homogeneity vectors as features

We built and tested a gradient-boosting classifier (GBM; with 300 estimators and learning rate = 0.1) model that predicts task-induced brain states using homogeneity vectors as features. With the k-fold cross-validation approach ($k = 10$ in this study), all the subjects are divided into k folds. At each iteration, the model was trained with all sessions of k-1 folds of subjects (9 sessions per subject) and then used to predict the task labels for the sessions of the remaining fold of subjects. (Fig. 1b) After N iterations, the predicted labels were compared to the true labels. The predictive power was evaluated by the mean predictive accuracy for each of the tasks, i.e., the proportion of correctly labels scans among all the scans whose true labels are task X, and the total accuracy. The accuracies range between 0% and 100% and higher accuracy indicates stronger predictive power. The importance of the homogeneity of each node for task classification is evaluated by the impurity-based feature importance extracted from the gradient-boosting classifier. The k-fold cross validation was repeated for 10 rounds. The mean and standard deviation of the accuracies are reported.

A permutation test was performed by randomly shuffling the task labels of the scans before building the gradient-boosting classifier and evaluating the predictive power in the same way as described above. Homogeneity vectors based on Shen 268 were used in the permutation test.

We also performed binary task classifications where each sample is labeled one of the two tasks rather than nine tasks. For each task pair, 986 samples (493 subjects * 2 sessions) were used for the same cross-validation and model building procedure. (Fig. 1c) A total of 36 (9 * (9–1)/2) accuracies for all task pairs were then computed and reported.

2.5. Sex classification using homogeneity vectors as features

The same gradient-boosting classifier model introduced in 2.4 was trained to classify subject sex based on homogeneity vectors. 211 male and 211 female subjects with matched age distributions were included. For each task, 422 scans were used for cross-validation and model training.

2.6. Statistical test comparing homogeneity distributions

For each node, the distributions of homogeneity across subjects under different states (tasks) are compared using paired *t*-test.

The distributions of mean homogeneity across subjects and states for different fixed atlases (Shen 268, Shen 368, and Yeo 1041) are compared using F test because the numbers of nodes are different for different parcellations. The distributions of mean homogeneity for fixed atlas (Shen 268), state-specific parcellation, and individualized parcellation are compared using paired *t*-test which is possible because this exemplar based parcellation maintains node correspondence across different parcellations.

2.7. Subject identification using homogeneity vectors

To identify the subject using a homogeneity vector, we first built a database containing homogeneity vectors for all subjects from task X. Then, the similarity between the target homogeneity vector from task Y and every vector in the database was evaluated. The predicted ID of the target vector would be the same as its most similar vector in the database. Here the similarity between vectors was evaluated by Pearson correlation. (Fig. 1d) A higher correlation coefficient r indicates higher similarity. The associated ID of each target vector was predicted independently, so multiple target vectors can be assigned the same ID although the true ID of every target vector from task Y is unique. A similar subject “fingerprinting” was performed in (Finn et al., 2015b) except that between-node connectivity was used as the feature in this previous study.

The task pairs used as the database and target are referred to as task X-task Y in Results and Discussion, e.g., REST-EMOTION means homogeneity vectors from REST are used as the database and homogeneity vectors from EMOTION are the targets whose ID are being predicted.

2.8. Between-voxel connectivity visualization

To better investigate the topography of voxel-to-voxel connectivity within a node, we randomly selected a seed voxel near the center of a node, for those nodes whose homogeneity was highly predictive for tasks. The seed-voxel to other voxels connectivity within the same node was calculated and visualized for different tasks to visualize within-node connectivity topology.

3. Results

In this work, homogeneity vectors containing the mean with-node connectivity for every node were obtained based on three fixed atlases at different resolution and used as features for task classification, sex classification, and subject identification. 493 subjects in the HCP dataset were used for task classification and subject identification. 422 subjects (211 males and 211 females) were used for sex classification. Homogeneity vectors based on individualized parcellations, state-specific parcellations and intersect parcellation were also used in the same classification and identification.

3.1. Task-induced brain states can be decoded from homogeneity vectors

Fig. 2a demonstrates that the gradient boosting classification model can predict, at high accuracy, task labels of scans based on homogeneity vectors. The task classification accuracies are essentially the same for the three atlases applied. The accuracy obtained from the permutation test where we randomly assign task labels to scans is very low and consistent with the theoretical probability by chance (1/9).

Fig. 2b shows the confusion matrix for multiclass task classification with Shen 268, i.e., what the true labels and predicted labels are for the misclassified scans. The major confusion was between REST and REST2. Among a total of 494 REST scans, 200 were misclassified as REST2, and similarly, 195 REST2 scans were misclassified as REST. Other relatively frequently misclassified task pairs include GAMBLING and RELATIONAL, EMOTION and GAMBLING, RELATIONAL, and WM, in the order of decreasing frequency.

The accuracies of binary task classifications for all task pairs are presented in Fig. 2c. The accuracy for REST vs. REST2 is 48% which is close to chance (50%). The accuracies for all the other task pairs are high and the lower ones among them are for GAMBLING vs. RELATIONAL, EMOTION vs. GAMBLING, RELATIONAL vs. WM, and REST2 vs. MOTOR. The task pairs with low binary classification accuracies are generally consistent with the pairs frequently get confused in multiclass classification.

3.2. Homogeneities of different nodes contribute unequally to task classification

To evaluate the importance of the homogeneity of each node, i.e., each element in the homogeneity vector for multiclass task classification, we used the impurity-based feature importance extracted from the classifiers. Fig. 3a shows the importance ranking of each node's homogeneity where the darker color represents higher importance. Fig. 3b summarizes the lobe distribution of the twenty most important nodes for task classification. Most of the nodes are in the occipital lobe (45%) followed by the temporal lobe (25%) and the parietal lobe (20%). A few nodes are in the motor strip (10%).

We plotted the distributions of homogeneities for the three most important nodes and three least important nodes under different tasks to further explore how homogeneities vary with states. (Fig. 3c) For the three most important nodes (left panel), the homogeneity distributions for REST (gray) are always significantly different from the distributions for other tasks at $p < 0.05$, except for Node 76, REST vs. REST2. Some of the distributions for REST and tasks are especially visually distinguishable, such as Node 209, REST vs. SOCIAL, Node 76 REST vs. RELATIONAL and WM. For the three least important nodes, most of the distributions for REST and tasks are still significantly different, but more non-significant cases are observed, and the p values are generally higher which means the significance levels are lower. It is also demonstrated in Fig. 3c that the homogeneities for the three most important nodes are higher than the three least important nodes.

We also performed the same task classification described in 3.1 with homogeneities of a subset of the nodes, rather than all 268 nodes. Fig. 3d shows the classification accuracies for each task and the total accuracy using homogeneity vectors containing the fifty most node homogeneities. The accuracies are comparable to the accuracies with complete homogeneity

vectors reported in Fig. 2a. However, with the fifty least important node homogeneities, the classification accuracies decrease considerably as shown in Fig. 3e Although the accuracies are still above chance.

3.3. Between-voxel connectivity varies with brain states which leads to homogeneity changes

As shown in Fig. 3c, the homogeneity of Node 209 is the most important feature for task classification and the homogeneity distributions are the most distinctive between REST and SOCIAL. To further investigate the between-voxel connectivity changes leading to such difference in homogeneity, we used one voxel in the center of Node 209 (marked in red in Fig. 4) as the seed voxel and correlated its timeseries to the timeseries of all the other voxels in Node 209. The correlation coefficients (functional connectivity) are shown in Fig. 4 for REST and SOCIAL. The result for a representative subject (subject 156,536) is presented here. Only a small local region around the seed voxel has high connectivity with the seed for REST, partly because no spatial smoothing was applied. However, for SOCIAL, many more voxels within the node have high connectivity with the node voxel. Such an increase in between-voxel functional connectivity during SOCIAL can lead to the significantly higher homogeneity observed in Fig. 3c.

3.4. Subject groups defined by sex can be distinguished based on homogeneity vectors

Fig. 5 demonstrates that using homogeneity as features, the gradient boosting classification model can classify sex at an accuracy much greater than chance. The classification accuracies, between 71% and 81%, are similar for all three atlases and all the tasks. The accuracies obtained from the random permutation test were approximately 50% as expected.

3.5. Subjects can be identified based on homogeneity vectors

We performed subject identification by evaluating the similarity of homogeneity vectors and quantified the accuracies of identification via these homogeneity vectors. (Fig. 6a) Three sets of homogeneity vectors based on different atlases were used respectively. The identification accuracy should always be 1 if the database homogeneity vectors and target homogeneity vectors are from the same task, so the diagonals of all three accuracy matrices are 1. For Shen 268 (left), using GAMBLING as the database and WM as the target yields the highest accuracy, followed by REST2-REST, REST-REST2, and RELATIONAL-WM. The accuracy ranges widely from 0.16 to 0.82. For Shen 368 (middle), the overall accuracy increases while the relative accuracy, i.e., which pairs yield higher accuracies, stays similar. The lowest accuracy is 0.38 and the highest accuracy reaches 0.96. For Yeo 1041 (right), the accuracies for all task pairs are high, between 0.89 and 1. There is a clear increase in subject identification accuracy as the number of nodes in the atlas, i.e., the number of elements in the homogeneity vector increases.

We further explored the reason for this increase in accuracy. Fig. 6b shows the distribution of correlation coefficients between homogeneity vectors from the same subject and different subjects. As the number of elements in homogeneity vectors increases, the standard deviations of the correlation coefficient between homogeneity vectors from the same subject and different subjects both decrease. Meanwhile, the correlation coefficient for

within-subject homogeneity vector pairs increases as the number of nodes increases from 268 to 368 and 368 to 1041 ($p < 0.001$). The correlation coefficient for between-subject homogeneity vector pairs is slightly higher for Shen 368 than for Shen 268 ($p < 0.001$) but is much lower for Yeo 1041 than both Shen 268 and Shen 368 ($p < 0.001$). In general, it is easier to distinguish between within-subject homogeneity pairs and between-subject homogeneity pairs as the number of nodes increases, which is consistent with the increase in identification accuracy in 5a.

The node homogeneity distributions for different atlases shown in Fig. 6c indicate that as the number of nodes increases and node size decreases, the node homogeneity increases. The homogeneities are averaged across subjects and states. However, there are still nodes with very low homogeneity scores when the number of nodes in the applied atlas is relatively high. In all cases the nodes are far from being functionally homogeneous, i.e., having homogeneities of 1, yet they are not simply noisy but have reliable patterns of connectivity within them that allow both brain-state (task) classification and subject identification.

3.6. Homogeneity vectors based on state-specific and individualized parcellations are still informative

Individualized parcellations obtained with the exemplar-based individualized parcellation method attempt to account for between-voxel connectivity changes within nodes across subjects and states by allowing node reconfiguration. Similarly, state-specific parcellations capture node reconfiguration only across states driven by changes in voxel-to-voxel connectivity. If the flexible parcellations were ideal they would yield completely homogeneous nodes, of the form that did not change with changes in brain state or group. To test this theory, we computed the homogeneity vectors based on state-specific and individualized parcellations and tested whether they still have predictive power for task-induced brain states and subject identity.

Fig. 7a shows the task classification accuracy using homogeneity vectors based on the fixed atlas (Shen 268), state-specific parcellations, and individualized parcellations. The accuracies for state-specific parcellations are about the same level as those for the fixed atlas. The accuracies decrease when homogeneity vectors based on individualized parcellations are used, especially for the tasks whose accuracies are the lowest among all the tasks (except for REST and REST2), GAMBLING, and RELATIONAL. Nonetheless, all the accuracies remain much higher than chance.

The subject identification accuracies using homogeneity vectors based on state-specific parcellations (Fig. 7b left) are very close to the accuracies for fixed atlas (Fig. 6a left). The accuracies for individualized parcellations (Fig. 7b right) are much lower than accuracies for the other two conditions.

We then compared the mean homogeneities across subjects and states based on different parcellation methods. Most of the data points representing homogeneities based on state-specific parcellations vs. fixed atlas (green dots in Fig. 8a left) sit around the unity line indicating that the differences between homogeneities based on fixed and state-specific parcellations are small (mean = 6.5×10^{-4}). The data points representing homogeneities

based on individualized parcellations vs. fixed atlas (red dots) are mostly above the unity line indicating that homogeneities based on individualized parcellations are generally higher than those based on fixed parcellations. The mean difference is 0.0124. The data points with darker colors represent homogeneities of nodes that are more important in task classification. The results suggest that the important nodes tend to have higher homogeneities, which is consistent with the observation in Fig. 4c. The right panel shows the distributions of homogeneities based on the three different parcellation methods. Node homogeneities based on state-specific parcellations and individualized parcellations are both higher than homogeneities based on fixed parcellations ($p < 0.001$) although the differences between fixed homogeneities and state-specific homogeneities are small.

Fig. 8b and 8c show that the distributions of the three node homogeneities most important for task-classification are shown for both state-specific parcellations and individualized parcellations are significantly different during REST and other tasks. Many of the distributions are visually distinct. This could be the reason for the relatively high task classification accuracies shown in Fig. 7a.

3.7. Homogeneity vectors based on intersect parcellation can be used for brain states decoding

Intercept parcellation contains only the voxels that are assigned to the same node across all nine state-specific parcellations. In Fig. 9a, the REST parcellation is used as the reference and the ratio between the number of voxels in intersect parcellation and the number of voxels in REST parcellation is reported for each node. The ratio ranges from 0.43 to 0.96 with a mean of 0.80. This indicates that most of the voxels are assigned to the same node across tasks.

To test whether the between-voxel connectivity of such a group of stably assigned voxels still has predictive power for tasks, we performed the same task classification based on homogeneity as described above. In this case, each node contains fewer voxels. Fig. 9b shows that the task classification accuracies remain high using homogeneity vectors based on the intersection of parcellations, comparable with the accuracies based on fixed atlas.

4. Discussion

4.1. Predictive power of within-node functional connectivity

Node homogeneity, which is the mean of the within-node functional connectivity, is a coarse metric. Yet, here we have shown that it can be used to classify tasks, distinguish groups according to sex, and identify subjects with high accuracy. These findings demonstrate that the functional connectivity within-nodes changes systematically with task-conditions and subject groups, and provides additional information unique to each subject. Within-node connectivity, co-varying with task or group is typically not measured nor controlled for in connectivity analyses. Detecting edge level connectivity changes in situations where the source of change may be within-node connectivity reconfigurations could provide an incomplete picture of the connectivity landscape, when contrasting groups or tasks.

There are several plausible reasons for the systematic changes in node homogeneity. The nodes in the most commonly used atlases may contain multiple distinctive, functional subunits that have specialized tunings, that vary with task. A simple biological explanation, that is completely compatible with a fixed structural infrastructure, can be centered around the number of neurons in a node. If the brain has the order of 16 billion neurons, then a 400-node atlas contains of the order of 40 million neurons. It is not a stretch to imagine that these neurons are not all tuned to the same inputs and outputs. Fine tuning of subsets of these millions of neurons likely supports sub-specialization of function within nodes and the resultant functional topography summarized by voxel time-courses varies as the task or brain state varies. There is significant literature of fine tuning at the individual neuron level to support this from the 2-photon literature (see for example (Barson et al., 2020)). Few studies have explicitly looked at within-node heterogeneity but using a fixed atlas in functional connectivity work assumes that all 40 million neurons in a node serve in the same functional role.

The standard approach of averaging the time series within the node not only obscures this potentially interesting within-node dynamic organization but can also distort the connectivity between nodes. One of the fixed atlases we applied, Yeo 1041 contains more nodes than most atlases. The homogeneities based on Yeo 1041 are higher than those based on atlases with fewer nodes. Yet, the task classification accuracy using homogeneity vectors based on this atlas is comparable to the accuracies based on the other two atlases and much higher than chance. This suggests that a 1041 node atlas still contains functional subunits and the functional topography within these nodes varies systematically with task. Given that functional organization in the brain is flexible (Salehi et al., 2020), and that functional units can be overlapping (Yeo et al., 2015), it is not clear that a fixed atlas at any scale would overcome this problem, except at the limit of course, treating each voxel as a node yields only 1 within-node time-course. Of course, there may be an atlas resolution between the 1041 node Yeo atlas that we used here and the approximately 85,000 $2mm^3$ voxels, but such an atlas has not been published to date. Incorporating stability of the within-node information between tasks in deriving a functional atlas may be a key to deriving a fixed atlas that works under all conditions.

Across all 3 atlases tested, the Shen 268, Shen 368, and Yeo 1041, the subject identification accuracy increases as the number of nodes increases likely because the number of features in the vector increases. In the limit of completely homogeneous nodes, there should be no information in the homogeneity vector, and subject identification accuracy should be at chance even if the atlas resolution is increased further.

4.2. Homogeneities based on flexible parcellations and the intersect parcellation

With state-specific parcellations, nodes are allowed to reconfigure, in a data driven manner, across different task-induced brain states. Individualized parcellations provide even more flexibility because each parcellation is derived for each subject and each state. However, the results show that the homogeneity vectors based on state-specific parcellations and individualized parcellations can still be used to predict tasks indicating that the variance in within-node connectivity across states is not fully accounted for by these flexible

parcellations (Fig. 7a). Subject identification accuracies are almost the same with fixed atlas and state-specific parcellations, suggesting that although the parcellation applied for each state is unique, the homogeneity patterns for different subjects are preserved. The subject identification accuracies based on individualized parcellations are lower than those based on the other two parcellation methods (Fig. 7b) possibly because allowing the parcellations to vary across subjects breaks the subject-specific patterns in homogeneity vectors. Individualized parcellations can also be noisier because they are based on a relatively small amount of data.

The information provided by within-node connectivity remains even with the state-specific and individualized parcellations possibly because of the restricted extent to which these parcellations are allowed to deviate from the initial fixed atlas and the coarse resolution (large node size). The exemplar-based individualized parcellation method preserves the node correspondence between individualized parcellations, which means the number of nodes is always held constant. The exemplar for each node is identified within the node in the initial fixed atlas and is usually near the geometric center of the node. In addition, the voxel-to-parcel assignment has a spatial contiguity constraint. Due to these restrictions, most of the voxels (~80%) around the geometric center of the nodes are consistently assigned to the same node across all state-specific parcellations. However, as shown in Fig. 4, the changes in connectivity within a node across states take place throughout the node. Such changes are not fully accounted for with the individualized parcellation method applied here.

To investigate performance of a parcellation that was consistent across tasks, we generated an intersect-parcellation, whose nodes contained only voxels that were consistently assigned to the same node across all state-specific parcellations. Each node in the intersect parcellation contains 43% to 96% of the voxels in the original REST state-specific parcellation, with a mean of 80% (Fig. 9b). The connectivity within-nodes in this intersect-parcellation however, still varies systematically across tasks, suggesting that an alternative approach is needed to fully account for these within-node connectivity changes.

4.3. Individualized parcellation methods account for inter-state and inter-subject differences

Studies have shown that there can be differences in the spatial configurations of nodes across subjects (Bijsterbosch et al., 2018) and individualized parcellation methods have been developed to attempt to account for these differences (Kong et al., 2019; Wang et al., 2015a). Methods have also been developed to compensate for both spatial differences between subjects as well as task-induced brain states (Boukhdhir et al., 2021; Salehi et al., 2020). Individualized parcellations have been shown to have higher functional homogeneity than fixed atlases (Kong et al., 2019; Salehi et al., 2020; Wang et al., 2015a). The subject-specific parcellations are relatively stable for the same subject and distinctive across different subjects (Wang et al., 2015a). Subtle differences in parcellations have been related to cognitive measures (Kong et al., 2019), and a metric extracted from subject-specific state-specific parcellations, the node size vector, has been shown to be useful in predicting task performance (Salehi et al., 2020).

The evidence strongly supports that functional spatial configurations vary systematically across subjects and states, yet the field has been slow to adapt to this functional flexibility. While the individualized atlas approaches attempt to accommodate functional reconfiguration, they do not achieve uniform state-independent homogeneity and sub-specialization within the individualized nodes remains. There is no consensus on which individualized parcellation method is the optimal and open questions remain as to the ideal number of nodes, and whether these should be contiguous. The change in homogeneity vector with task could be added as a constraint to a parcellation algorithm, where parcel size is decreased until the within-node connectivity between tasks stabilizes. Here we tested the implicit assumption of the fixed atlas approach that the node can be treated as a homogeneous unit, and we demonstrate that significant changes in connectivity occur within-nodes in a reliable manner. The work here does not demonstrate, nor argue, that one atlas is better than another. However, it does indicate that the use of a fixed atlas when studying changes in connectivity across brain states or groups, overlooks significant within node changes in connectivity. Such changes occur even with atlases of up to 1000 nodes, which is a higher resolution than found in most studies.

4.4. Implications

Almost all studies to date have used atlases with hard boundaries and employed the same atlas across all subjects and, in studies where task data is included, all task-conditions. The underlying assumption has been that the node acts as a cohesive unit and that within-node connectivity is high, constant, and therefore not of interest. The homogeneity measure used in this work is only a coarse metric to measure the extent to which voxels within a node share the same temporal dynamics across scan conditions. This coarse measure however contains sufficient information to allow task classification (gradient boosting classifier), classification of subjects by sex, and subject identification (correlation-based fingerprinting), and yet these are by no means the optimal models to extract information on within node connectivity changes. The results suggest that a considerable amount of information on the connectivity topology is missed when only edge changes are considered. A danger in not considering within node connectivity changes is that such changes may be incorrectly ascribed to external edge changes leading to incorrect interpretation of the connectivity changes observed.

Although state-specific parcellations have previously been shown to reflect dynamic brain functional organization (Salehi et al., 2020), the results here show that they do not fully account for changes in within-node connectivity to yield completely homogeneous parcellations that do not vary systematically with task or group. However, there are several potential directions for future works.

First, increasing the number of nodes in the atlas does lead to higher within-node functional similarity. Since one possible reason for the systematic changes in node homogeneity is the mixing and matching of different functional subunits within a node, further dividing the nodes to separate these subunits provides a potential solution. However, it remains an open question whether there exist spatially contiguous units that are consistently functionally synchronized under all states at the current scale of neuroimaging. It is shown in this

work that parcellations with as many as 1041 nodes are not fine enough to ensure stable within-node connectivity. Previous work (Salehi et al., 2020) has revealed consistent and predictive reconfiguration for parcellations containing even 5000 nodes. Thus, if there exists a fixed atlas that meets the previously described assumption, it is likely to require even more than 5000 nodes.

Allowing more flexible parcellations is another potential way to better account for within-node connectivity variance. Current approaches to flexible parcellation hold the number of nodes fixed and limit the amount of reconfiguration allowed to maintain node correspondence. It is currently unknown however, if the number, size, and location of functional units varies substantially across subjects and brain states. However, to compare connectomes across individuals and tasks requires node correspondence across all these conditions. Thus, it can be challenging to find the balance between these competing goals for parcellation.

For some analyses, metrics derived from within-node connectivity, such as homogeneity, could be included as separate factors. For example, homogeneity vectors can be included as an additional set of input variables when building models to predict behavior from connectivity (Finn et al., 2015a; Shen et al., 2017). It is not straightforward however to incorporate metrics such as homogeneity in direct contrasts of connectivity matrices or networks. Even if this is not achievable, at a minimum, the variance of within-node connectivity should not be correlated with the variable of interest when examining connectivity changes. For example, if one were to investigate differences in node-level functional connectivity between task-induced states, within-node connectivity should not vary systematically with task-induced states. This study, however, demonstrates that using current methods it does co-vary with the variables of interest.

Other approaches such as ICA analyses (Iraji et al., 2019, 2020; Smith et al., 2013b; Tian et al., 2013) or gradient approaches partially avoid the parcellation problem and yield components that can be analyzed in a manner similar to the parcellation based connectome. ICA can provide multiple spatially overlapping components and these can be allowed to vary with condition. These ICA components are often few in number (30–70) and may not be spatially contiguous and share more in common with network analyses rather than node analyses (Salehi et al., 2018; Smith et al., 2011). In the gradient work (Margulies et al., 2016; Vázquez-Rodríguez et al., 2019) principal axes have been investigated and in some cases these have been shown to vary with task (Tian et al., 2020). ICA has also shown spatial modulation of components as a function of task (Calhoun et al., 2008). Both the ICA and gradient approaches are promising avenues for untangling the organizing principles of the brain supporting behavior. They differ from atlas- based approaches primarily in terms of how the circuits are localized.

Finally, if we consider an atlas only as a tool for dimension reduction, then simply performing the analyses on voxel-level connectivity rather than node-level connectivity mostly avoids the challenge of choosing the appropriate parcellation. Note that a 2 mm^3 voxel contains on the order of ~200,000 neurons and thus there could be considerable sub-specialization within a voxel – we just can’t see it because the voxel is our smallest

unit of measure. Previous studies have investigated voxel-level connectivity analysis (Hayasaka and Laurienti, 2010; Wang et al., 2015b), and some metrics based on voxel-level connectivity have been proposed to prevent the high computational expense of full voxel-level connectivity analyses (Scheinost et al., 2012).

5. Conclusions

In this work, we demonstrate that connectivity between voxels within-nodes varies systematically and predictively across subjects and task-induced brain states. Almost all functional connectivity studies to date have used fixed parcellations across a range of conditions or groups, focusing only on changes in node-to-node connectivity while ignoring within-node connectivity changes, which are shown here to be informative. Such changes in within-node connectivity may be misinterpreted as edge changes leading to erroneous conclusions. The results are shown to replicate across three different fixed atlases covering resolutions from 268 to over 1000 nodes. Several potential strategies can be adopted to account for the within-node connectivity changes and make use of this additional information when studying connectivity changes between groups and/or different task conditions and brain states.

Supplementary Material

Refer to Web version on PubMed Central for supplementary material.

Acknowledgement

Support from NIH MH121095 is gratefully acknowledged

References

Antoniou IE, Tsompa ET, 2008. Statistical analysis of weighted networks. Discrete Dyn. Nat. Soc 2008, 375452.

Barson D, Hamodi AS, Shen X, Lur G, Constable RT, Cardin JA, Crair MC, Higley MJ, 2020. Simultaneous mesoscopic and two-photon imaging of neuronal activity in cortical circuits. Nat. Methods 17, 107–113. [PubMed: 31686040]

Bijsterbosch JD, Woolrich MW, Glasser MF, Robinson EC, Beckmann CF, Van Essen DC, Harrison SJ, Smith SM, 2018. The relationship between spatial configuration and functional connectivity of brain regions. Elife 7, e32992. [PubMed: 29451491]

Biswal B, Yetkin FZ, Haughton VM, Hyde JS, 1995. Functional connectivity in the motor cortex of resting human brain using echo-planar MRI. Magn. Reson. Med 34, 537–541. [PubMed: 8524021]

Blumensath T, Jbabdi S, Glasser MF, Van Essen DC, Ugurbil K, Behrens TE, Smith SM, 2013. Spatially constrained hierarchical parcellation of the brain with resting-state fMRI. Neuroimage 76, 313–324. [PubMed: 23523803]

Bolaños M, Bernat EM, He B, Aviyente S, 2013. A weighted small world network measure for assessing functional connectivity. J. Neurosci. Methods 212, 133–142. [PubMed: 23085279]

Boukhdhir A, Zhang Y, Mignotte M, Bellec P, 2021. Unraveling reproducible dynamic states of individual brain functional parcellation. Network Neurosci. 5, 28–55.

Bozek J, Makropoulos A, Schuh A, Fitzgibbon S, Wright R, Glasser MF, Coalson TS, O'Muircheartaigh J, Hutter J, Price AN, 2018. Construction of a neonatal cortical surface atlas using multimodal surface matching in the developing human connectome project. Neuroimage 179, 11–29. [PubMed: 29890325]

Brodmann K, 1909. Vergleichende Lokalisationslehre der Großhirnrinde: in ihren Prinzipien dargestellt auf Grund des Zellenbaues. Barth JA, Leipzig.

Calhoun VD, Kiehl KA, Pearlson GD, 2008. Modulation of temporally coherent brain networks estimated using ICA at rest and during cognitive tasks. Hum. Brain Mapp 29, 828–838. [PubMed: 18438867]

Caviness VS Jr, Meyer J, Makris N, Kennedy DN, 1996. MRI-based topographic parcellation of human neocortex: an anatomically specified method with estimate of reliability. J. Cogn. Neurosci 8, 566–587. [PubMed: 23961985]

Cohen JR, D'Esposito M, 2016. The segregation and integration of distinct brain networks and their relationship to cognition. J. Neurosci 36, 12083–12094. [PubMed: 27903719]

Eickhoff SB, Constable RT, Yeo BT, 2018. Topographic organization of the cerebral cortex and brain cartography. Neuroimage 170, 332–347. [PubMed: 28219775]

Fan L, Li H, Zhuo J, Zhang Y, Wang J, Chen L, Yang Z, Chu C, Xie S, Laird AR, 2016. The human brainnetome atlas: a new brain atlas based on connectional architecture. Cerebral Cortex 26, 3508–3526. [PubMed: 27230218]

Finn ES, Shen X, Scheinost D, Rosenberg MD, Huang J, Chun MM, Papademetris X, Constable RT, 2015a. Functional connectome fingerprinting: identifying individuals using patterns of brain connectivity. Nat. Neurosci 18, 1664–1671. [PubMed: 26457551]

Finn ES, Shen X, Scheinost D, Rosenberg MD, Huang J, Chun MM, Papademetris X, Constable RT, 2015b. Functional connectome fingerprinting: identifying individuals using patterns of brain connectivity. Nat. Neurosci 18, 1664–1671. [PubMed: 26457551]

Geerligs L, Renken RJ, Saliasi E, Maurits NM, Lorist MM, 2015. A brain-wide study of age-related changes in functional connectivity. Cereb Cortex 25, 1987–1999. [PubMed: 24532319]

Glasser MF, Coalson TS, Robinson EC, Hacker CD, Harwell J, Yacoub E, Ugurbil K, Andersson J, Beckmann CF, Jenkinson M, 2016. A multi-modal parcellation of human cerebral cortex. Nature 536, 171–178. [PubMed: 27437579]

Glasser MF, Sotiropoulos SN, Wilson JA, Coalson TS, Fischl B, Andersson JL, Xu J, Jbabdi S, Webster M, Polimeni JR, Van Essen DC, Jenkinson M, Consortium WU-MH, 2013. The minimal preprocessing pipelines for the human connectome project. Neuroimage 80, 105–124. [PubMed: 23668970]

Gordon EM, Laumann TO, Adeyemo B, Huckins JF, Kelley WM, Petersen SE, 2016. Generation and evaluation of a cortical area parcellation from resting-state correlations. Cerebral Cortex 26, 288–303. [PubMed: 25316338]

Hayasaka S, Laurienti PJ, 2010. Comparison of characteristics between region-and voxel-based network analyses in resting-state fMRI data. Neuroimage 50, 499–508. [PubMed: 20026219]

Iraji A, Deramus TP, Lewis N, Yaesoubi M, Stephen JM, Erhardt E, Belger A, Ford JM, McEwen S, Mathalon DH, Mueller BA, Pearlson GD, Potkin SG, Preda A, Turner JA, Vaidya JG, van Erp TGM, Calhoun VD, 2019. The spatial chronnectome reveals a dynamic interplay between functional segregation and integration. Hum. Brain Mapp 40, 3058–3077. [PubMed: 30884018]

Iraji A, Miller R, Adali T, Calhoun VD, 2020. Space: a missing piece of the dynamic puzzle. Trends Cogn Sci 24, 135–149. [PubMed: 31983607]

Joshi A, Scheinost D, Okuda H, Belhachemi D, Murphy I, Staib LH, Papademetris X, 2011. Unified framework for development, deployment and robust testing of neuroimaging algorithms. Neuroinformatics 9, 69–84. [PubMed: 21249532]

Kong R, Li J, Orban C, Sabuncu MR, Liu H, Schaefer A, Sun N, Zuo X-N, Holmes AJ, Eickhoff SB, 2019. Spatial topography of individual-specific cortical networks predicts human cognition, personality, and emotion. Cerebral Cortex 29, 2533–2551. [PubMed: 29878084]

Lacadie CM, Fulbright RK, Rajeevan N, Constable RT, Papademetris X, 2008. More accurate Talairach coordinates for neuroimaging using non-linear registration. Neuroimage 42, 717–725. [PubMed: 18572418]

Lawrence RM, Bridgeford EW, Myers PE, Arvapalli GC, Ramachandran SC, Pisner DA, Frank PF, Lemmer AD, Nikolaidis A, Vogelstein JT, 2021. Standardizing human brain parcellations. Sci Data 8, 1–9. [PubMed: 33414438]

Lord A, Ehrlich S, Borchardt V, Geisler D, Seidel M, Huber S, Murr J, Walter M, 2016. Brain parcellation choice affects disease-related topology differences increasingly from global to local network levels. Psychiatry Res. 249, 12–19.

Luo W, Greene AS, Constable RT, 2021. Within node connectivity changes, not simply edge changes, influence graph theory measures in functional connectivity studies of the brain. Neuroimage, 118332. [PubMed: 34224851]

Ma S, Calhoun VD, Phlypo R, Adalı T, 2014. Dynamic changes of spatial functional network connectivity in healthy individuals and schizophrenia patients using independent vector analysis. Neuroimage 90, 196–206. [PubMed: 24418507]

Margulies DS, Ghosh SS, Goulas A, Falkiewicz M, Huntenburg JM, Langs G, Bezgin G, Eickhoff SB, Castellanos FX, Petrides M, Jefferies E, Smallwood J, 2016. Situating the default-mode network along a principal gradient of macroscale cortical organization. Proc. Natl. Acad. Sci 113, 12574–12579. [PubMed: 27791099]

McIntosh AR, 2004. Contexts and catalysts: a resolution of the localization and integration of function in the brain. Neuroinformatics 2, 175–182. [PubMed: 15319515]

Messé A, 2020. Parcellation influence on the connectivity-based structure–function relationship in the human brain. Hum. Brain Mapp 41, 1167–1180. [PubMed: 31746083]

Meunier D, Achard S, Morcom A, Bullmore E, 2009. Age-related changes in modular organization of human brain functional networks. Neuroimage 44, 715–723. [PubMed: 19027073]

Park B, Ko JH, Lee JD, Park H-J, 2013. Evaluation of node-inhomogeneity effects on the functional brain network properties using an anatomy-constrained hierarchical brain parcellation. PLoS ONE 8, e74935. [PubMed: 24058640]

Power JD, Cohen AL, Nelson SM, Wig GS, Barnes KA, Church JA, Vogel AC, Laumann TO, Miezin FM, Schlaggar BL, 2011. Functional network organization of the human brain. Neuron 72, 665–678. [PubMed: 22099467]

Qi S, Meesters S, Nicolay K, ter Haar Romeny BM, Ossenblok P, 2015. The influence of construction methodology on structural brain network measures: a review. J. Neurosci. Methods 253, 170–182. [PubMed: 26129743]

Rolls ET, Huang C-C, Lin C-P, Feng J, Joliot M, 2020. Automated anatomical labelling atlas 3. Neuroimage 206, 116189. [PubMed: 31521825]

Rosenberg MD, Finn ES, Scheinost D, Constable RT, Chun MM, 2017. Characterizing attention with predictive network models. Trends Cogn Sci 21, 290–302. [PubMed: 28238605]

Rosenberg MD, Finn ES, Scheinost D, Papademetris X, Shen X, Constable RT, Chun MM, 2016. A neuromarker of sustained attention from whole-brain functional connectivity. Nat. Neurosci 19, 165–171. [PubMed: 26595653]

Rosenberg MD, Scheinost D, Greene AS, Avery EW, Kwon YH, Finn ES, Ramani R, Qiu M, Constable RT, Chun MM, 2020. Functional connectivity predicts changes in attention observed across minutes, days, and months. Proc. Natl. Acad. Sci. USA 117, 3797–3807. [PubMed: 32019892]

Rubinov M, Sporns O, 2010. Complex network measures of brain connectivity: uses and interpretations. Neuroimage 52, 1059–1069. [PubMed: 19819337]

Rudie JD, Brown J, Beck-Pancer D, Hernandez L, Dennis E, Thompson P, Bookheimer S, Dapretto M, 2013. Altered functional and structural brain network organization in autism. NeuroImage 2, 79–94.

Salehi M, Greene AS, Karbasi A, Shen X, Scheinost D, Constable RT, 2020. There is no single functional atlas even for a single individual: functional parcel definitions change with task. Neuroimage 208, 116366. [PubMed: 31740342]

Salehi M, Karbasi A, Barron DS, Scheinost D, Constable RT, 2018. State-specific individualized functional networks form a predictive signature of brain state. bioRxiv.

Santarnecchi E, Emmendorfer A, Tadayon S, Rossi S, Rossi A, Pascual-Leone A, 2017. Network connectivity correlates of variability in fluid intelligence performance. Intelligence 65, 35–47.

Satterthwaite TD, Wolf DH, Roalf DR, Ruparel K, Erus G, Vandekar S, Gennatas ED, Elliott MA, Smith A, Hakonarson H, Verma R, Davatzikos C, Gur RE, Gur RC, 2015. Linked sex differences

in cognition and functional connectivity in youth. Cereb Cortex 25, 2383–2394. [PubMed: 24646613]

Schaefer A, Kong R, Gordon EM, Laumann TO, Zuo X-N, Holmes AJ, Eickhoff SB, Yeo BT, 2018. Local-global parcellation of the human cerebral cortex from intrinsic functional connectivity MRI. Cerebral Cortex 28, 3095–3114. [PubMed: 28981612]

Scheinost D, Benjamin J, Lacadie C, Vohr B, Schneider KC, Ment LR, Papademetris X, Constable RT, 2012. The intrinsic connectivity distribution: a novel contrast measure reflecting voxel level functional connectivity. Neuroimage 62, 1510–1519. [PubMed: 22659477]

Shen X, Finn ES, Scheinost D, Rosenberg MD, Chun MM, Papademetris X, Constable RT, 2017. Using connectome-based predictive modeling to predict individual behavior from brain connectivity. Nat. Protoc 12, 506–518. [PubMed: 28182017]

Shen X, Tokoglu F, Papademetris X, Constable RT, 2013. Groupwise whole-brain parcellation from resting-state fMRI data for network node identification. Neuroimage 82, 403–415. [PubMed: 23747961]

Shine JM, Bissett PG, Bell PT, Koyejo O, Balsters JH, Gorgolewski KJ, Moodie CA, Poldrack RA, 2016. The dynamics of functional brain networks: integrated network states during cognitive task performance. Neuron 92, 544–554. [PubMed: 27693256]

Smith SM, Miller KL, Salimi-Khorshidi G, Webster M, Beckmann CF, Nichols TE, Ramsey JD, Woolrich MW, 2011. Network modelling methods for FMRI. Neuroimage 54, 875–891. [PubMed: 20817103]

Smith SM, Vidaurre D, Beckmann CF, Glasser MF, Jenkinson M, Miller KL, Nichols TE, Robinson EC, Salimi-Khorshidi G, Woolrich MW, Barch DM, Ugurbil K, Van Essen DC, 2013a. Functional connectomics from resting-state fMRI. Trends Cogn Sci 17, 666–682. [PubMed: 24238796]

Smith SM, Vidaurre D, Beckmann CF, Glasser MF, Jenkinson M, Miller KL, Nichols TE, Robinson EC, Salimi-Khorshidi G, Woolrich MW, Barch DM, Uğurbil K, Van Essen DC, 2013b. Functional connectomics from resting-state fMRI. Trends Cogn. Sci 17, 666–682. [PubMed: 24238796]

Sporns O, Tononi G, Kötter R, 2005. The human connectome: a structural description of the human brain. PLoS Comput. Biol 1, 0245–0251.

Tian L, Kong Y, Ren J, Varoquaux G, Zang Y, Smith SM, 2013. Spatial vs. temporal features in ica of resting-state fMRI - A quantitative and qualitative investigation in the context of response inhibition. PLoS ONE 8, e66572. [PubMed: 23825545]

Tian L, Wang J, Yan C, He Y, 2011. Hemisphere-and gender-related differences in small-world brain networks: a resting-state functional MRI study. Neuroimage 54, 191–202. [PubMed: 20688177]

Tian Y, Margulies DS, Breakspear M, Zalesky A, 2020. Topographic organization of the human subcortex unveiled with functional connectivity gradients. Nat Neurosci 1–12. [PubMed: 31844312]

Vázquez-Rodríguez B, Suárez LE, Markello RD, Shafiei G, Paquola C, Hagmann P, van den Heuvel MP, Bernhardt BC, Spreng RN, Misic B, 2019. Gradients of structure–function tethering across neocortex. Proc. Natl. Acad. Sci 116, 21219–21227. [PubMed: 31570622]

Wang D, Buckner RL, Fox MD, Holt DJ, Holmes AJ, Stoecklein S, Langs G, Pan R, Qian T, Li K, Baker JT, Stufflebeam SM, Wang K, Wang X, Hong B, Liu H, 2015a. Parcellating cortical functional networks in individuals. Nat. Neurosci 18, 1853–1860. [PubMed: 26551545]

Wang Y, Cohen JD, Li K, Turk-Browne NB, 2015b. Full correlation matrix analysis (FCMA): an unbiased method for task-related functional connectivity. J. Neurosci. Methods 251, 108–119. [PubMed: 26004849]

Yeo BT, Krienen FM, Eickhoff SB, Yaakub SN, Fox PT, Buckner RL, Asplund CL, Chee MW, 2015. Functional specialization and flexibility in human association cortex. Cereb Cortex 25, 3654–3672. [PubMed: 25249407]

Yeo BT, Krienen FM, Sepulcre J, Sabuncu MR, Lashkari D, Hollinshead M, Roffman JL, Smoller JW, Zöllei L, Polimeni JR, 2011. The organization of the human cerebral cortex estimated by intrinsic functional connectivity. J. Neurophysiol.

Zhang C, Cahill ND, Arbabshirani MR, White T, Baum SA, Michael AM, 2016. Sex and age effects of functional connectivity in early adulthood. Brain Connect 6, 700–713. [PubMed: 27527561]

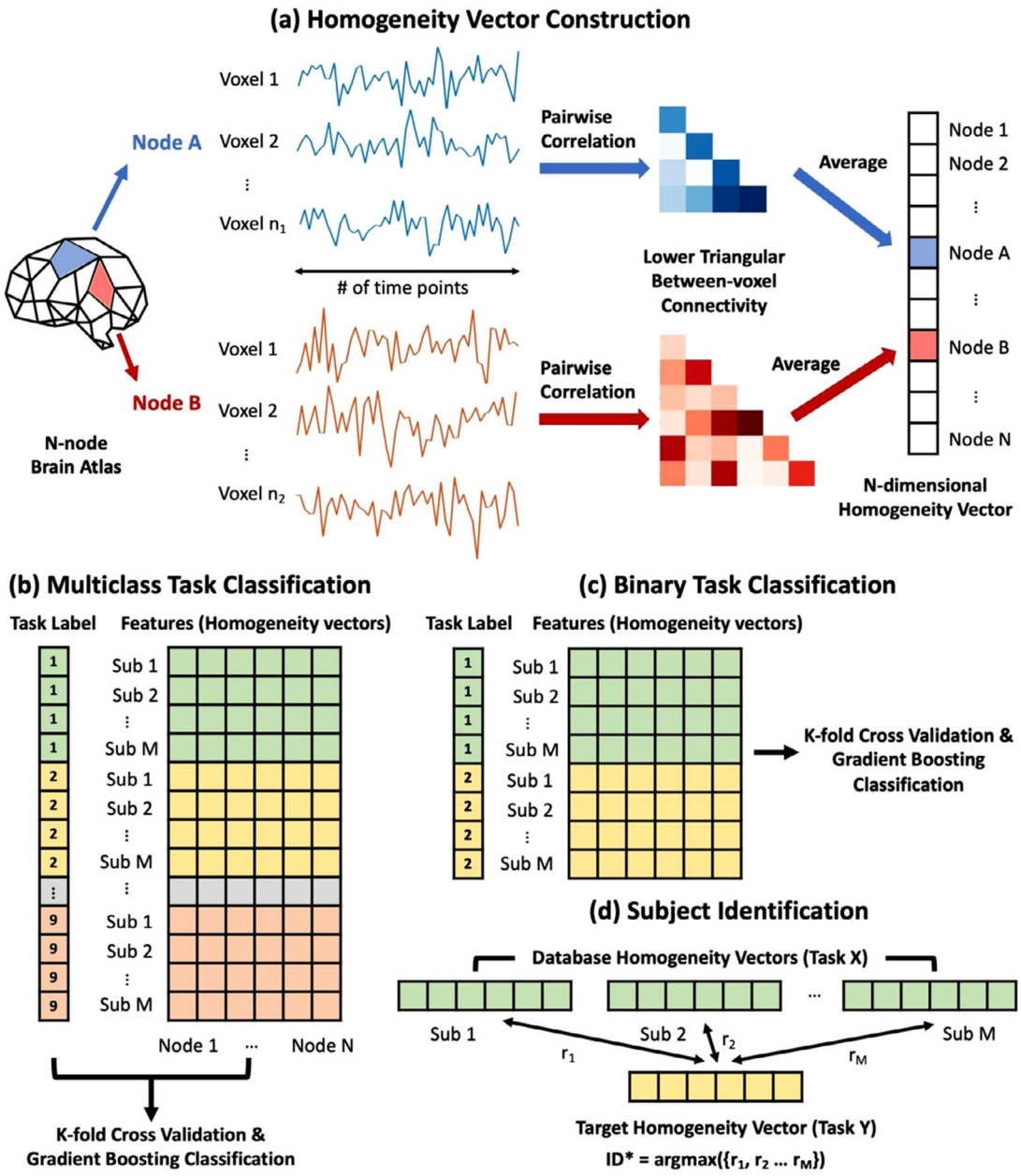

Fig. 1.

(a) The homogeneity of each node is defined as the mean pair-wise correlation between voxel-level time series within the node. The within-node between-voxel connectivity matrices can have different sizes because the nodes can contain different numbers of voxels. There is a homogeneity vector associated with each scan which contains the homogeneities of all the nodes defined by the atlas applied. The number of elements in the homogeneity vector is the same as the number of nodes in the atlas applied. (b) Each scan is considered as one entry. The scans are labeled 1 to 9 depending on the task performed during the scans. All the entries (493 subjects * 9 sessions) are divided into k folds. At each iteration, a gradient-boosting classifier was trained with k-1 folds and then used to predict the task labels for the remaining fold. (c) Binary task classification is almost the same as

multiclass task classification in (b) except that only scans from two different tasks are being distinguished each time. (d) To identify the subject using a homogeneity vector, we first built a database containing homogeneity vectors for all subjects from task X. Then, the similarity between the target homogeneity vector from task Y and every vector in the database was evaluated. The predicted ID of the target vector would be the same as its most similar vector in the database. Here the similarity between vectors was evaluated by Pearson correlation.

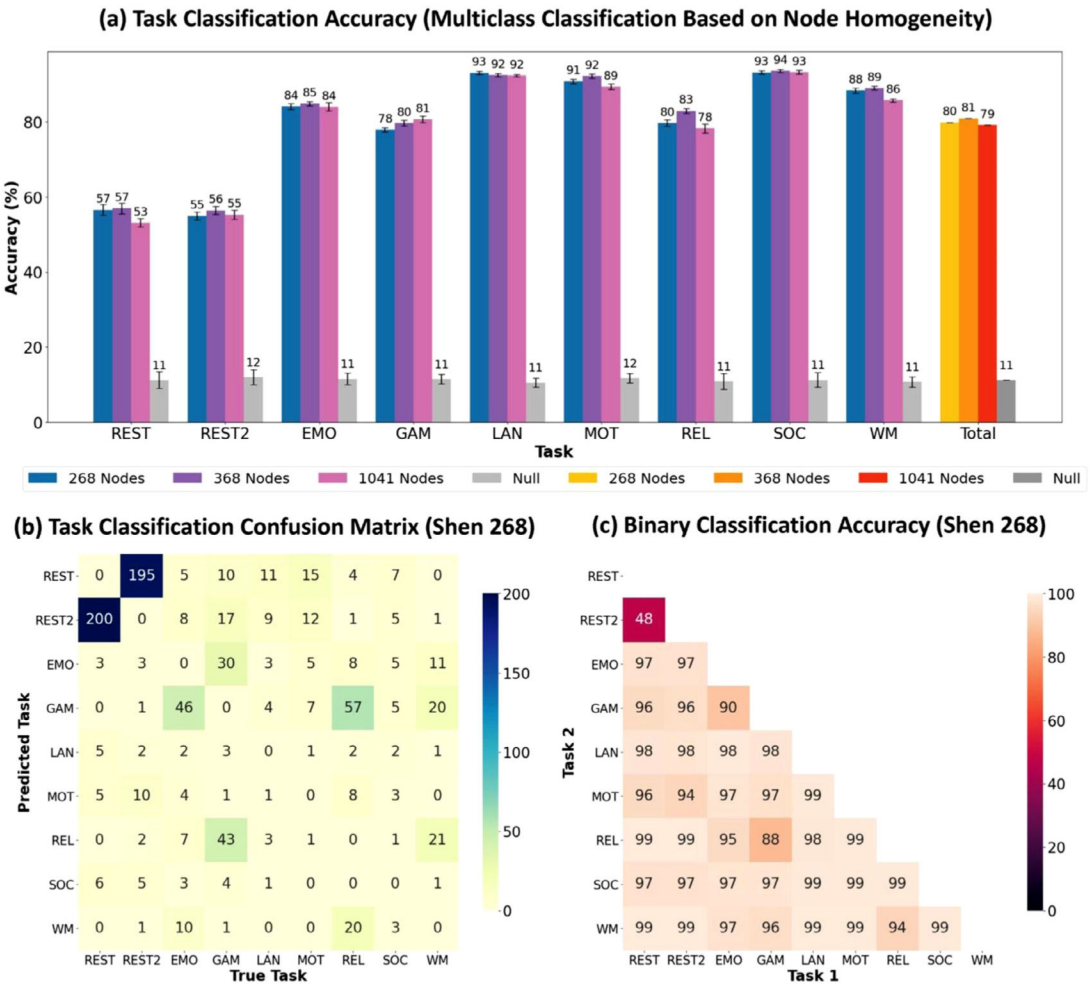

Fig. 2.

(a) The mean task classification accuracies across 10 repetitions for each task (the scans whose true labels are this particular task) and the total classification accuracy. The accuracies for three different parcellations, Shen 268, Shen 368, and Yeo 1041 are reported in different colors. The gray bars represent the accuracies obtained from the permutation test where the labels are randomly assigned to the scans. The standard deviations are indicated with the error bars. (b) The confusion matrix for task classification based on Shen 268. The numbers represent the number of scans whose true labels are shown on the x axis but are misclassified as the task on the y axis. Darker color means more misclassified scans. (c) The accuracies for binary task classification. Darker color means lower classification accuracy, i.e., more misclassified scans.

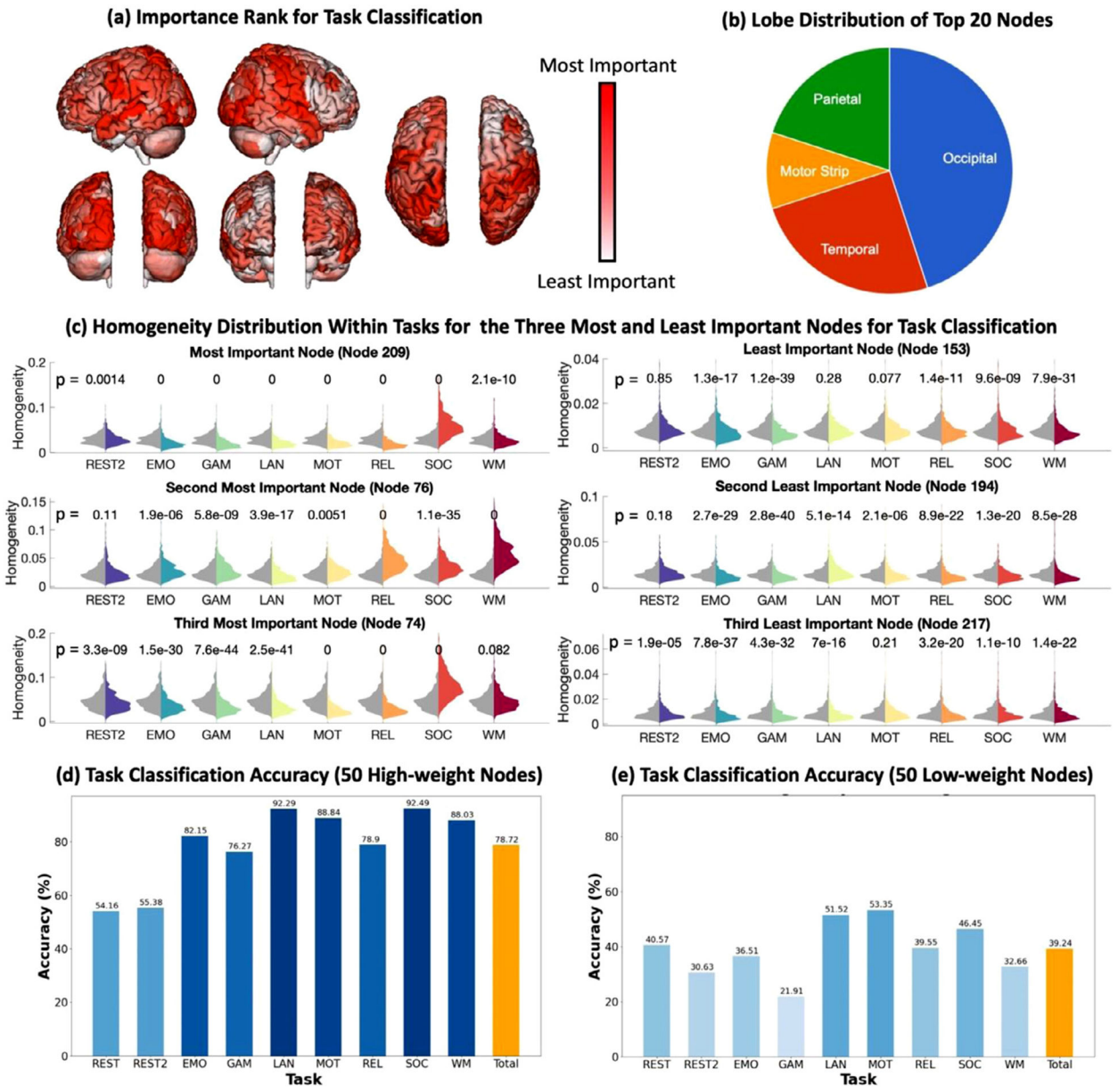

Fig. 3.

(a) The importance ranking of each node's homogeneity for multiclass task classification. The darker color represents higher importance. (b) The lobe distribution of the twenty most important nodes for task classification. (c) The distributions of homogeneities for the three most important nodes and three least important nodes for multiclass task classification under different tasks. The gray distributions show the homogeneities under REST for 493 subjects and the distributions in other colors represent the homogeneities under other tasks labeled on the x axis. Paired *t*-test was used to compare the homogeneity distributions under REST and tasks. The p values are reported (above each pair of distribution). (d) The multiclass task classification accuracies for each task and the total accuracy using homogeneity vectors containing the fifty most node homogeneities. (e) The multiclass task

classification accuracies for each task and the total accuracy using homogeneity vectors containing the fifty least node homogeneities.

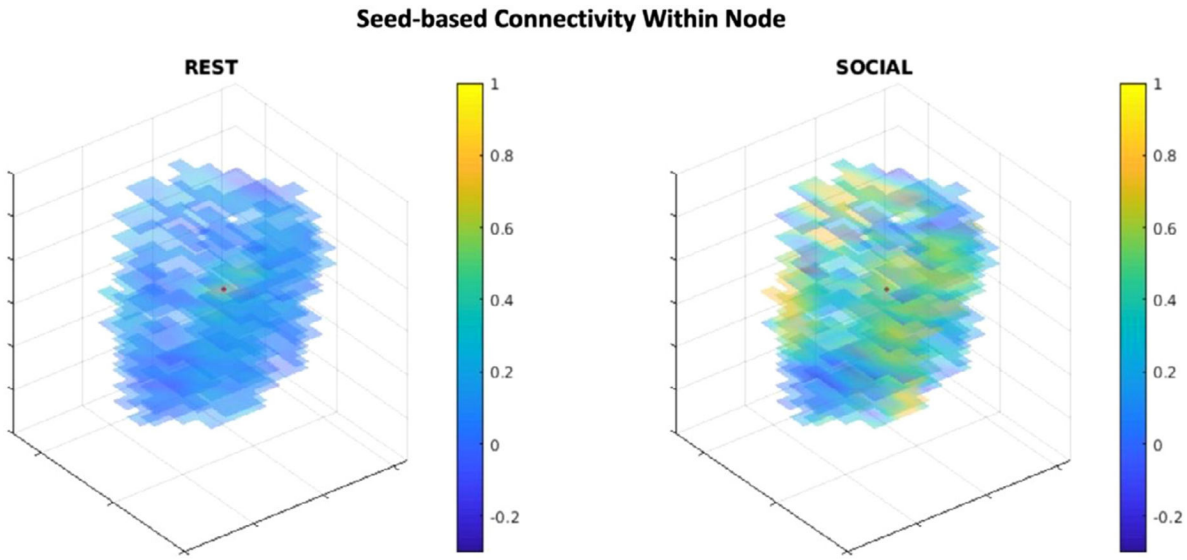

Fig. 4.

The between-voxel connectivity within Node 209 for subject 156,536 under REST and SOCIAL. The seed voxel is marked by the red dot. The color of other voxels represents the functional connectivity between the voxel and the seed.

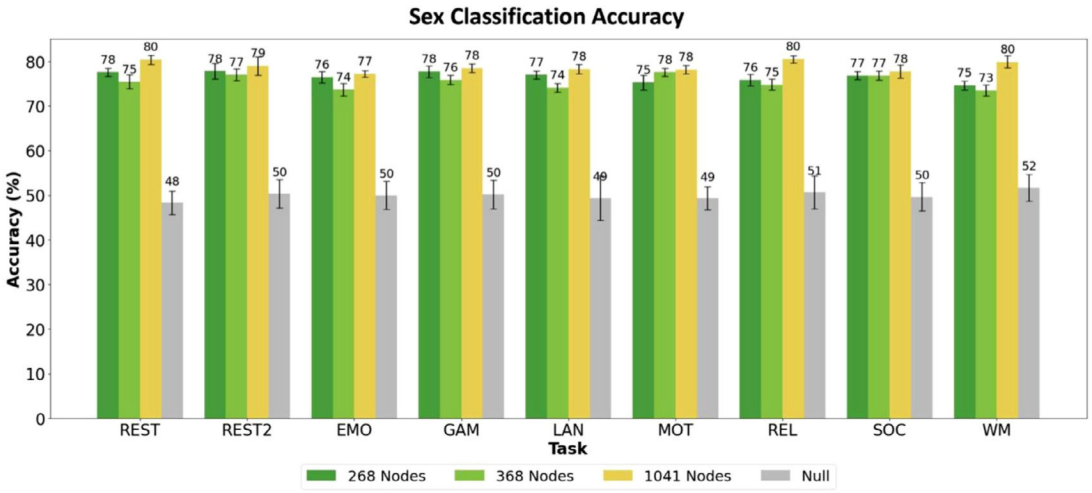

Fig. 5.

The mean sex classification accuracies across 10 repetitions for each task. Separate sex classification models were built and tested for each task with scans from 211 male and 211 female subjects. The accuracies for three different parcellations, Shen 268, Shen 368, and Yeo 1041 are reported in different colors. The gray bars represent the accuracies obtained from the permutation test where the sex labels are shuffled. The standard deviations are indicated with the error bars.

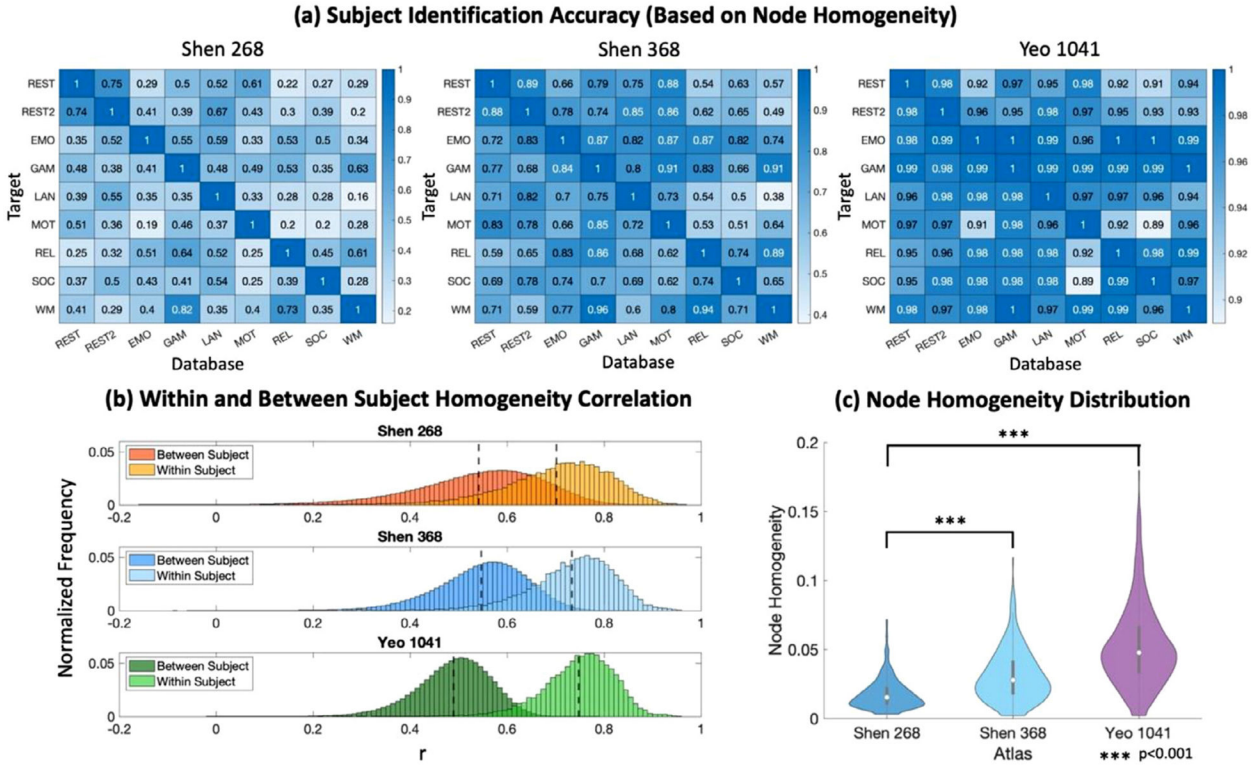

Fig. 6.

(a) The subject identification accuracies using homogeneity vectors based on Shen 268, Shen 368, and Yeo 1041. The x axis shows homogeneity vectors from which task are used as the database (Task X shown in Fig. 1d) and the y axis shows homogeneity vectors from which task are used as the targets. The identification accuracy should always be 1 if the database homogeneity vectors and target homogeneity vectors are from the same task, so the diagonals of all three accuracy matrices are 1. Darker color represents higher accuracy. (b) The distribution of correlation coefficients between homogeneity vectors from the same subject and different subjects. (c) The distribution of node homogeneity for different atlases. The homogeneity for each node is averaged across subjects and states. The distributions are compared with F test.

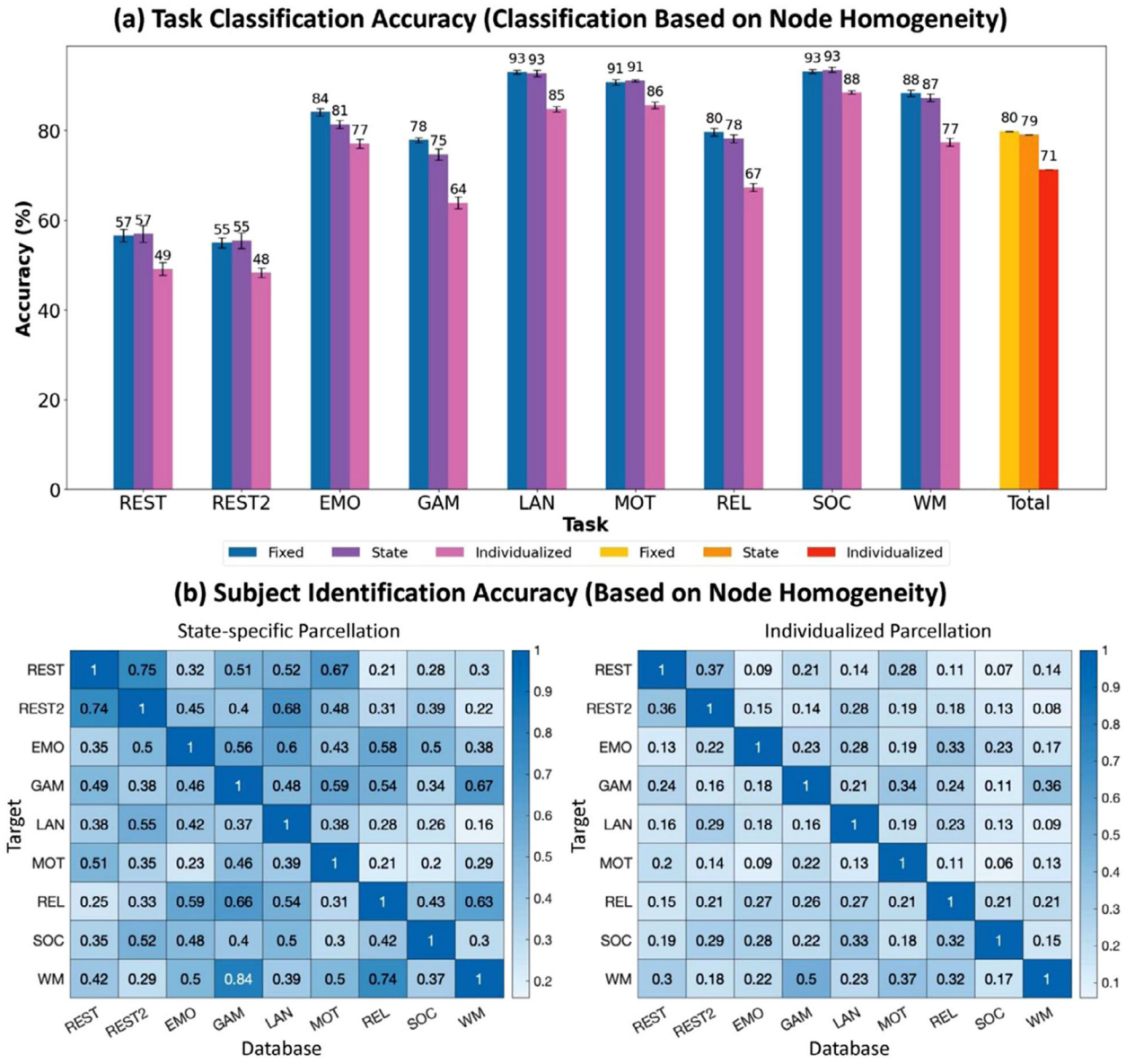

Fig. 7.

(a) The mean multiclass task classification accuracy across 10 repetitions using homogeneity vectors based on the fixed atlas (Shen 268), state-specific parcellations, and individualized parcellations. The standard deviations are indicated with the error bars. (b) The subject identification accuracies using homogeneity vectors based on state-specific parcellations and individualized parcellations.

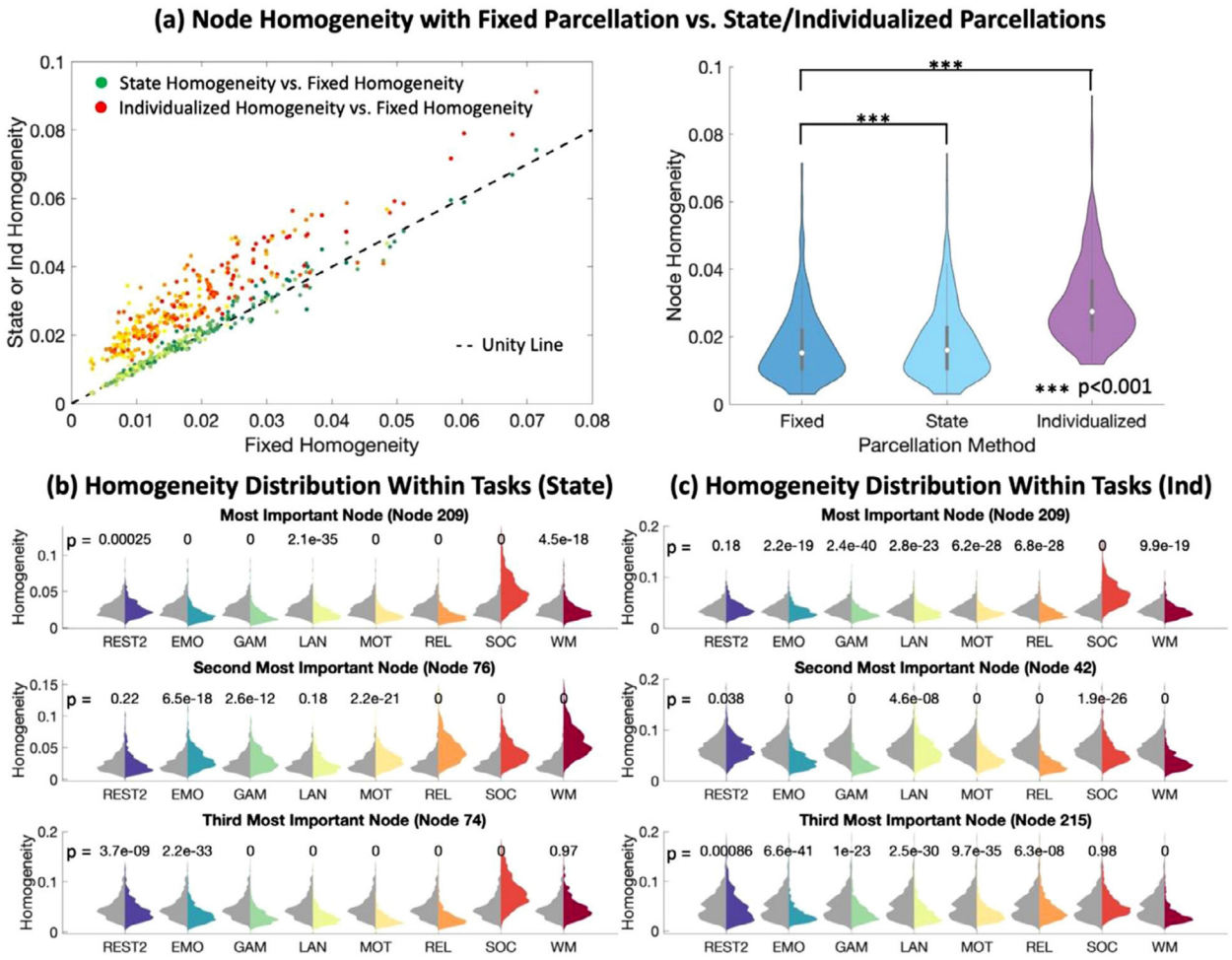

Fig. 8.

(a) Left panel: The green distribution shows the mean node homogeneity across subjects and states based on state-specific parcellations vs. fixed atlas (Shen 268). The orange distribution shows the mean node homogeneity based on individualized parcellations vs. fixed atlas. The dashed line is the unity line on which the homogeneities based on state-specific parcellations or individualized parcellations are the same as the homogeneities based on the fixed atlas. Right panel: The distribution of node homogeneity for fixed atlas, state-specific parcellations, and individualized parcellations. The homogeneity for each node is averaged across subjects and states. The distributions are compared with paired t-tests. (b) The homogeneity distributions based on state-specific parcellations for the three most important nodes (for task classification) are shown for all task conditions. The gray distributions represent the homogeneity distributions for REST for 493 subjects and are provided for reference, while the distributions in the other colors represent the homogeneities under tasks labeled on the x axis. Paired t-tests were used to compare the homogeneity distributions under REST and tasks. The p values are reported (above each pair of distribution). (c) The distributions of homogeneities based on individualized parcellations for the three most important nodes under different tasks.

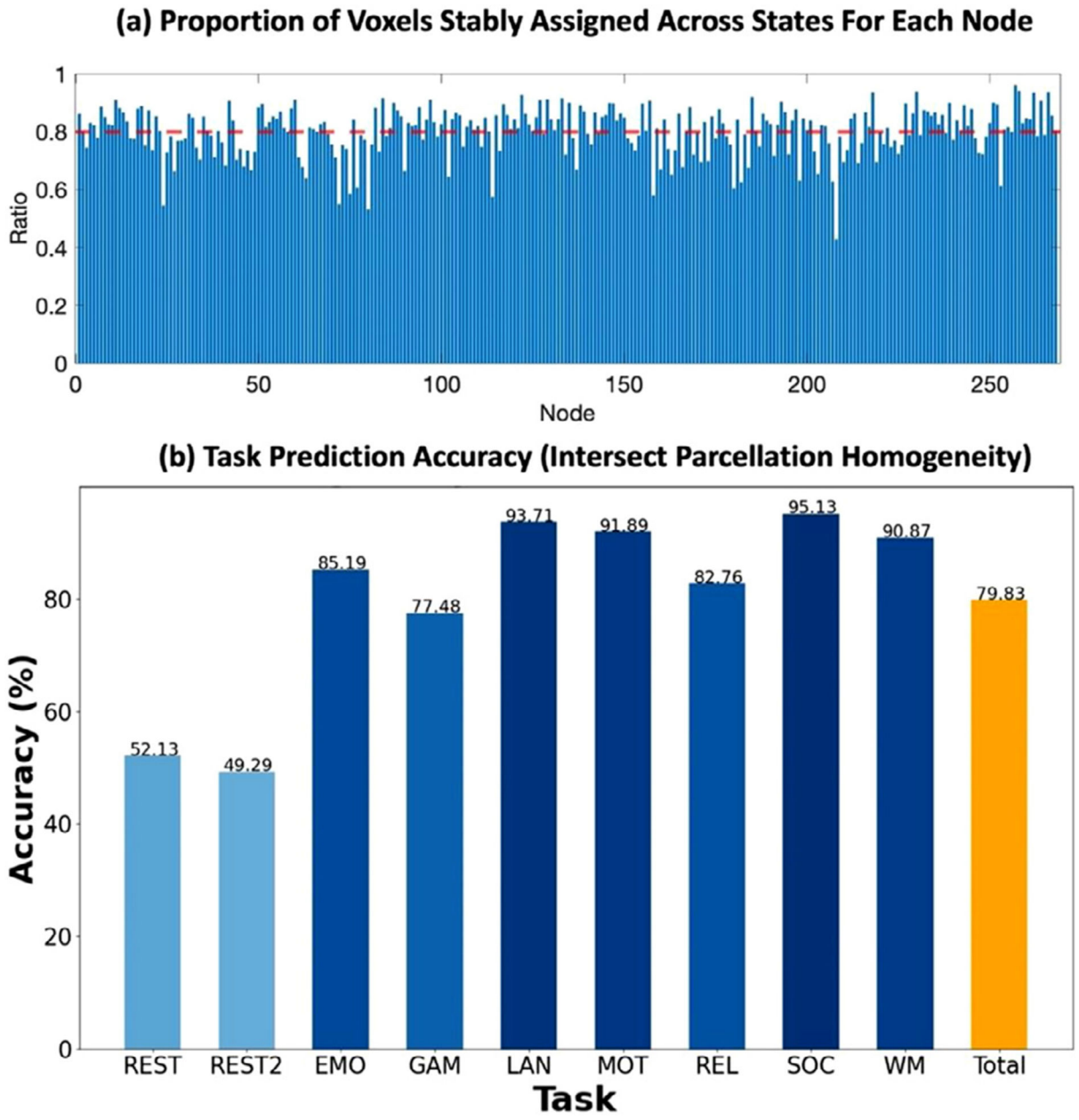

Fig. 9.

(a) The proportion of voxels stably assigned to the same node across all states among all voxels for each node in REST state-specific parcellation, i.e., the ratio between node size in the intersect parcellation and REST state-specific parcellation. The red dashed line shows the mean ratio across all the nodes. (b) The multiclass task classification accuracies for each task and the total accuracy using homogeneity vectors based on the intersect parcellation.